MRO-CRISM 2006-2008 MARTIAN CLOUD MAP RETRIEVALS.

D. R. Klassen, *(klassen@rowan.edu)*, **B. D. West,** *Rowan University, New Jersey, USA*.

Introduction

There in an inherent difficulty in the visible wavelength (VIS) and near-infrared (NIR) when one moves from a technique of tracking cloud positions and getting semi-quantitative relative thicknesses to retrieving full optical depth measurements that is much less problematic in other wavebands such as ultraviolet (UV) and thermal infrared (TIR); namely in the VIS-NIR one needs to properly characterize the intrinsic surface reflectance in order to complete the radiative transfer modeling. Since the spectra are not easily separable into surface and aerosol components, there are two primary techniques one can use to get an approximate surface spectrum: find your region of interest on another day you believe to be free of cloud cover and use the retrieved spectrum as the surface, or find another "nearby" region in the same image that appears to be similar enough to your region of interest and appears free of cloud cover and use that spectrum as the surface proxy. Neither of these is usable if one is going to scale up the cloud measurements to the entire globe of Mars. Additionally, the first idea requires that the surface reflectance remain relatively static in time while the second requires surface reflectance to vary slowly across a scene of interest.

For the past several years we have been working on devising and improving a technique to retrieve surface reflectance spectral signatures without any a priori assumptions about the non-variability of the surface itself. Our only assumption is that all surfaces can be decomposed into a finite set of constant spectral endmembers. While we have seen limited success on our ground-based data (due primarily to significant variation in signal-to-noise and various calibration difficulties) we have begun to see promise on spacecraft-based data.

In this paper we will briefly outline the technique and present retrieved cloud optical depth maps that will span an entire martian year and discuss their validity relative to the current understanding of major cloud cycles.

The Data

We used NIR spectral data taken by the Compact Reconnaissance Imaging Spectrometer for Mars (CRISM) in its multi-spectral mapping mode. This mode collects data in only 74 wavelengths using subsets of wavelengths from both of its gratings so the spectra nominally cover the range 0.362–3.920 μm. In this mode the frame rate of data collection was 15 to 30 Hz along track and spectra are binned 5:1 or 10:1 cross-track giving a spatial resolution of about 100 or 200 m (Murchie & CRISM Team, 2007).

For this work we took spectra from about 20 days in order to build a (still rather sparse) mapped image cube (longitude by latitude by wavelength). Spectra were averaged down to a spatial resolution of $1/8^\circ \times 1/8^\circ$ in order to reduce the number of points to make computation feasible. We also reduced the spectral range down to 1.559–3.9235 μm, leaving out the martian atmospheric CO_2 band between 1.875–2.139 μm which tends to confuse the surface recovery technique (Klassen, 2016). So far we have created 6 such maps that span a martian year; details on these image cubes are in table 1.

To compute the surface spectral endmembers we created a seventh image cube by zonally averaging each day of input data then stacking the resulting latitude by wavelength sets to make a latitude by date by wavelength image cube. Doing this allows us to run the surface recovery technique across all times but reduces the spatial information to a more manageable size.

Surface Endmember Recovery

In order to pull out the most spectrally "pure" surface endmembers we used a multi-step process: principal components analysis (PCA) to map the spectra into a new space based on the internal variation of the data which also reduces the dimensionality of the problem (Klassen et al., 1999; Klassen, 2016), target transformation (TT) to map target mineral spectra in the PC-space and expand the data cloud (Bandfield et al., 2000); construct the smallest volume around the resulting cloud using a combination of the Quickhull (Barber et al., 1996) and N-FINDR (Winter, 1999) algorithms; Hyperplane-based Craig Simplex Identification (HyperCSI) (Lin et al., 2016) to expand that volume until it has only $N + 1$ vertices around the cloud in the reduced N-dimensional space.

While PCA is good at finding in-data differences and "traits", Klassen & Bell (2001) showed that it was not enough to pull out purely surface endmembers. The TT method on top of that is meant to expand the data cloud by adding spectra that are conceivable surface materials, thereby emphasizing the directions in the PC-space that correspond to surfaces and minimize the effect of non-linear and non-surface spectral traits. For this work, the surface targets are from the *MRO CRISM Spectral Library* (CRISM Spectral Library Working Group, 2006) from the Planetary Data System (PDS). The Quickhull algorithm reduces the number of endmember candidates

Table 1: CRISM Image Cube Information

Name	Start Date – End Date	# of Days	Median L_S
2006_321	08 NOV 2006 – 25 NOV 2006	18	136.7°
2007_071	01 MAR 2007 – 30 MAR 2007	22	198.8°
2007_170	04 JUN 2007 – 03 JUL 2007	30	260.6°
2007_261	08 SEP 2007 – 28 SEP 2007	21	316.0°
2008_012	28 DEC 2007 – 27 JAN 2008	31	016.4°
2008_167	31 MAY 2008 – 25 JUN 2008	21	085.6°
L_S-map	image of L_S by latitude with each day zonally averaged		

by finding only those that reside on the data cloud "surface" while N-FINDR then searches those points for $N + 1$ vertices that maximize the total volume about the data cloud. The final step, HyperCSI inflates those vertices to create the N-dimensional hyper-tetrahedron. The vertices of this figure are then the "most pure" spectral endmembers in a space defined by the data variation and all possible surface minerals.

Cloud Optical Depth Calculation

With the recovered surface endmember spectra now known, the measurement of cloud optical depth is simply a matter of creating a test spectrum from a radiative transfer model, using ice and dust optical depth and coefficients to linearly combine the endmembers and vary those seven parameters until a least-squares best fit between model and data is found. This is done for each point, in each map.

The radiative transfer program used was that of Wolff et al. (2009) which was built upon the DISORT subroutines (Stamnes et al., 1988). The program inputs include the incidence, emission, and phase angles for each point—reduced to the image set average for simplicity; a dust cloud particle effective size ($r_{\text{eff}} = 1.5\,\mu\text{m}$), effective size distribution variance ($\nu_{\text{eff}} = 0.4$), and radiative phase function (from Tomasko et al., 1999); an ice cloud particle effective size ($r_{\text{eff}} = 2.0\,\mu\text{m}$), effective variance ($\nu_{\text{eff}} = 0.1$), and radiative phase function (from Clancy et al., 2003); and vertical profiles of pressure and temperature. The program uses the 41-layer profiles from MGS-TES ick 1629–163.

In practice, running the model for each point in each map through a full error minimization is computationally prohibitive so we adopted the technique of Wolff et al. (2011) wherein we make a set of models over a reasonable range of all seven parameters and use this as a sort of look-up table—that is we simply look for the best fit between the data and this subset of possible models and then record the cloud optical depth for that point and move on.

The resulting cloud optical depth maps are presented in figure 1.

Results & Discusion

As we start our sequence in northern summer (figure 1a) the largest optical depths are over the Tharsis peaks and Alba Patera and the aphelion cloud belt (ACB) is apparent with optical depth about 0.20–0.30. The ACB then disappears first followed later by the loss of orographic clouds as perihelion approaches (figures 1b and 1c).

With the recession of the north polar cap we see clouds in the far north (figure 1d) with optical depths less than about 0.20 at the edge of Utopia in the east and Acidalia in the center and by northern spring (figure 1e) those northern clouds have thickened to greater than 0.25 with the increase in available water vapor.

Finally (figure 1f) we are back to early northern summer and, while significantly sparser in data than the other maps, we can just make out orographic clouds and hints of the ACB.

Quantitatively, we can compare optical depths within the ACB to other studies. At its height in the 2006_321 map we see $0.2 \leq \tau_{12.1\,\mu\text{m}} < 0.3$; Smith (2004) measured zonally averaged ice TIR optical depth of ≥ 0.15 with MGS-TES and Mateshvili et al. (2009) measure zonally averaged ice UV optical depth at 0.3–0.4 in the cloud belt latitudes at similar L_S. All of these results appear to be generally consistent.

While we see great promise here in that we can create cloud maps with optical depths that are in agreement with previous results, we do note that there is some aliasing in the maps—the calculation of clouds over particularly dark regions seems to fail.

We have also not presented any dust optical depth maps as it turns out those are not giving reasonable values—the best fit matching seems to break down at trying to distinguish between bright regions with thin dust clouds and instead returns them as dark areas with bright dust above them. We believe this is in part because there is great spectral similarity between bright regions and dust. We are investigating methods of restricting results based on dust optical depth to see if that will work better.

Finally, we have several more CRISM data files we can process into maps, redo the endmember recovery, and perhaps find some distinctions that will help in both of these issues.

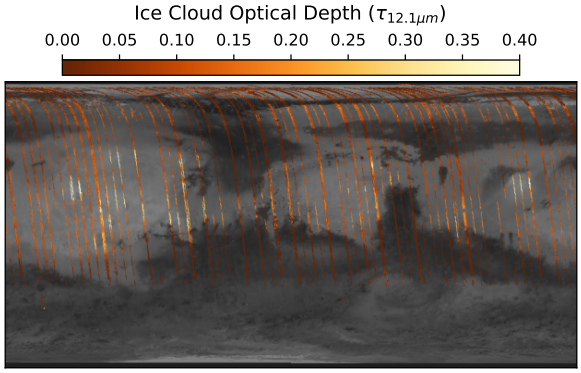

(a) 2006_321

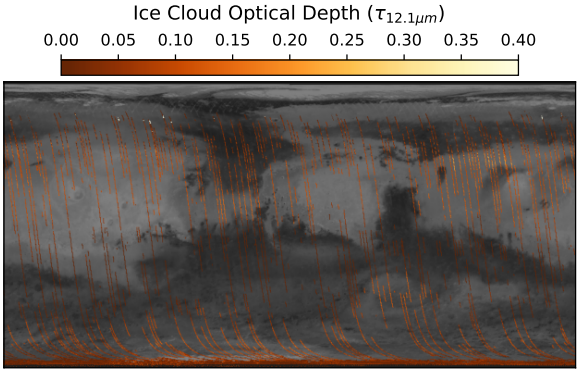

(d) 2007_261

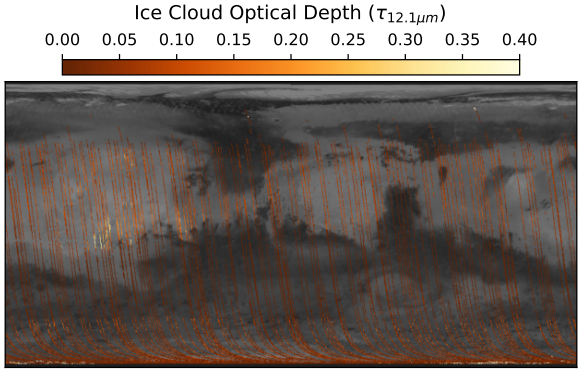

(b) 2007_071

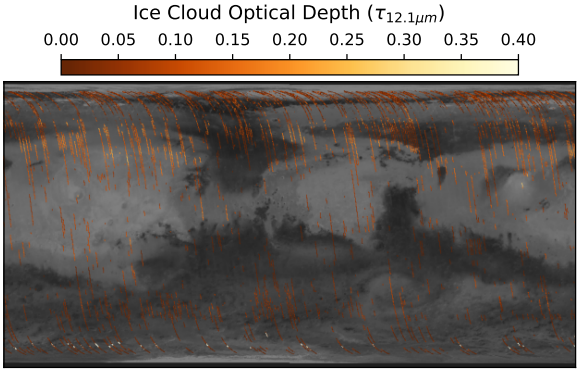

(e) 2008_012

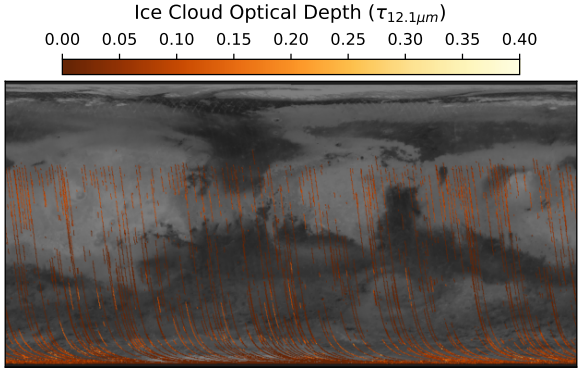

(c) 2007_170

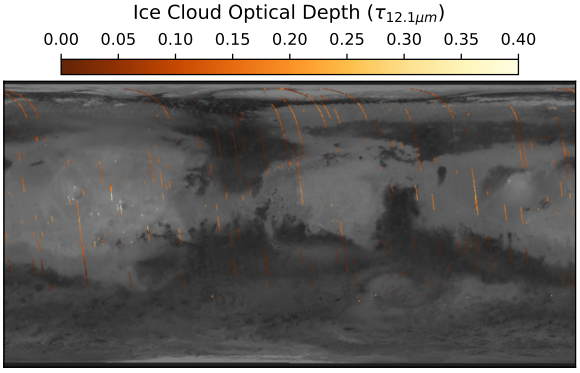

(f) 2008_167

Figure 1: Ice cloud optical depth maps for the six spectral image cubes; all τ-maps are presented on the same color scale from $0 < \tau < 0.4$ for clearer comparison.

Figure 1: -continued- Ice cloud optical depth maps for the six spectral image cubes; all τ-maps are presented on the same color scale from $0 < \tau < 0.4$ for clearer comparison.

References

Bandfield, J. L., Christensen, P. R., & Smith, M. D. (2000). Spectral data set factor analysis and end-member recovery: Application to analysis of Martian atmospheric particulates. *J. Geophys. Res.*, 105, 9573–9588.

Barber, C. B., Dobkin, D. P., & Huhdanpaa, H. (1996). The quickhull algorithm for convex hulls. *ACM Trans. Math. Softw.*, 22(4), 469–483.

Clancy, R. T., Wolff, M. J., & Christensen, P. R. (2003). Mars aerosol studies with the MGS TES emission phase function observations: Optical depths, particle sizes, and ice cloud types versus latitude and solar longitude. *J. Geophys. Res. Plan.*, 108, 2–1.

CRISM Spectral Library Working Group (2006). The MRO CRISM Spectral Library. https://pds-geosciences.wustl.edu/missions/mro/spectral_library.htm.

Klassen, D. R. (2016). Principal components analysis of martian nir image cubes to retrieve surface spectral endmembers. *Publications of the Astronomical Society of the Pacific*, 128(965), 074501.

Klassen, D. R. & Bell, J. F. (2001). Principal Components Analysis Studies of Martian Clouds. *Bull. Amer. Astron. Soc.*, 33, 1069–1070.

Klassen, D. R., Bell, J. F., Howell, R. R., Johnson, P. E., Golisch, W., Kaminski, C. D., & Griep, D. (1999). Infrared Spectral Imaging of Martian Clouds and Ices. *Icarus*, 138, 36–48.

Lin, C., Chi, C., Wang, Y., & Chan, T. (2016). A fast hyperplane-based minimum-volume enclosing simplex algorithm for blind hyperspectral unmixing. *IEEE Transactions on Signal Processing*, 64(8), 1946–1961.

Mateshvili, N., Fussen, D., Vanhellemont, F., Bingen, C., Dekemper, E., Loodts, N., & Tetard, C. (2009). Water ice clouds in the Martian atmosphere: Two Martian years of SPICAM nadir UV measurements. *Planet. Space Sci.*, 57, 1022–1031.

Murchie, S. & CRISM Team (2007). Compact Reconnaissance Imaging Spectrometer for Mars (CRISM) on Mars Reconnaissance Orbiter (MRO). *J. Geophys. Res. Plan.*, 112(E11), 5.

Smith, M. D. (2004). Interannual variability in TES atmospheric observations of Mars during 1999-2003. *Icarus*, 167, 148–165.

Stamnes, K., Tsay, S.-C., Jayaweera, K., & Wiscombe, W. (1988). Numerically stable algorithm for discrete-ordinate-method radiative transfer in multiple scattering and emitting layered media. *Appl. Optics*, 27, 2502–2509.

Tomasko, M. G., Doose, L. R., Lemmon, M., Smith, P. H., & Wegryn, E. (1999). Properties of dust in the Martian atmosphere from the Imager on Mars Pathfinder. *J. Geophys. Res.*, 104, 8987–9008.

Winter, M. E. (1999). N-FINDR: an algorithm for fast autonomous spectral end-member determination in hyperspectral data. In M. R. Descour & S. S. Shen (Eds.), *Imaging Spectrometry V*, volume 3753 of *Proc. SPIE* (pp. 266–275).

Wolff, M. J., Clancy, R. T., Cantor, B., & Madeleine, J.-B. (2011). Mapping Water Ice Clouds (and Ozone) with MRO/MARCI. In F. Forget & E. Millour (Ed.), *Mars Atmosphere: Modelling and observation* (pp. 213–216).

Wolff, M. J., Smith, M. D., Clancy, R. T., Arvidson, R., Kahre, M., Seelos, F., Murchie, S., & Savijärvi, H. (2009). Wavelength dependence of dust aerosol single scattering albedo as observed by the Compact Reconnaissance Imaging Spectrometer. *J. Geophys. Res. Plan.*, 114(E13), E00D04.